



Numerical Simulations of the Cabbeling Phenomenon in Surface Gravity Currents in Cold Fresh Water

Alabodite Meipre George ^{a*} and Anthony Kay ^b

^aDepartment of Mathematics and Computer Science, Niger Delta University, Wilberforce Island, Bayelsa State, Nigeria.

^bDepartment of Mathematical Sciences, Loughborough University, Loughborough, Leicestershire, LE11 3TU, United Kingdom.

Authors' contributions

This work was carried out in collaboration between both authors. Both authors read and approved the final manuscript.

Article Information

DOI: 10.9734/JSRR/2022/v28i130488

Open Peer Review History:

This journal follows the Advanced Open Peer Review policy. Identity of the Reviewers, Editor(s) and additional Reviewers, peer review comments, different versions of the manuscript, comments of the editors, etc are available here: <https://www.sdiarticle5.com/review-history/83005>

Received 01 December 2021

Accepted 03 February 2022

Published 05 February 2022

Original Research Article

ABSTRACT

The behaviour of warm water discharge at a temperature higher than T_m horizontally into a homogeneous body of cold fresh water at a temperature lower than T_m was investigated by means of a numerical model. Water density here was taken to be a quadratic function of temperature. Thus cabbeling process was inevitable as positively buoyant water form surface current while penetrating the ambient water. The current halted as mixture became dense and sink. These results are very similar to the experimental study of warm discharge into cold water by Marmoush et al. [14] and Bukreev [22]. The results showed an initially sinking water at the point where the two water bodies meets within the first few time interval. Development of Rayleigh-Taylor instabilities was observed at the lower part of the surface current as lighter fluid penetrate further. The frontal head was found to being replenished by a surface flow of warm unadulterated water, but after much entrainment of ambient fluid and cabbeling then, this head halted and sink. On the floor, denser fluid advance in the same direction as the original surface current, with some degree of Kelvin-Helmholtz instability as it penetrates further. Relations were also drawn that describes the speed, the spread length of both surface current were obtained.

*Corresponding author: E-mail: alaboditemgeorge@ndu.edu.ng, georgianalgebra@gmail.com;

Relation were also drawn that describes the final spread length of the surface current L_{sm} and the time taken to reach that final spread length τ_{sm} as a function ϕ_{in} . This work as presented here is practical and relevant to many fields of study and also enhances policy making towards the protection of the aquatic ecosystems.

Keywords: Surface current; cabbeling; temperature of maximum density.

1 INTRODUCTION

The motion of fluids with temperatures on either sides of the temperature of maximum density T_m , initially at rest but separated by a vertical barrier in a rectangular domain was studied. Where the value $3.98^\circ C$ is the T_m for fresh water at atmospheric pressure, (i.e., approximately $4^\circ C$ in some numerical calculation). After the removal of such a barrier, it is known that difference in the hydrostatic pressure causes the denser fluid to flow in one direction either to the left or to the right hand side along the floor. While the lighter fluid flows in the opposite direction along the top, which create a mixing region between the two fluids as they interact with each other. Thus, this behaviour is as a result of the density gradients due to temperature differences. The occurrence of this phenomenon is always frequent in nature or from human intervention. For instance, thunderstorm outflows and sea-breeze fronts are gravity currents, driven by difference in temperature and the oceanic fronts resulting from the difference in temperature and salinity. Gravity currents can also be observed as a result of differences in particulate suspension, such as volcanic pyroclastic flows, snow avalanches and turbidity currents in the ocean, where suspended particles play a major role in density gradients. [1, 2, 3].

There have been several analysis on this phenomenal behaviour from lock-exchange over rough and smooth horizontal surfaces. Where the analysis in those of the currents over a rough horizontal surfaces can be found in [3], and flows through forest canopies can also be found in [4, 5]. And some of such flows through urban canopies are found in [6, 7, 8]. Where all these is focused more in the rate of entrainment, drag and dispersion due to bottom roughness or the obstacles encountered during the current flow; which is beyond the scope of this paper.

Whereas, in the case for gravity current flows using the lock-exchange configuration over a smooth horizontal bottom, this have also been studied experimentally, theoretically and numerically. Earlier theoretical investigations of gravity current with this configuration predict that the front speed of these currents decrease as $t^{-1/3}$, with the assumption that the motion is determined mainly by a balance between inertia and buoyancy of the fluid in the current [9, 10, 11, 12]. Hacker et al. [13] experimentally studied the behaviour of density currents, and observed the occurrence of a substantial mixing phase within the early stages of the lock release. And this later led to the formation of a complex internal density structure as Kelvin-Helmholtz mode and rolls up. Fluid detrained from the head is always replaced by dense fluid from the rear, and a sharp moving head is maintained as the current spread further on the floor of the domain. Lastly was a region of stratified fluid (mixed fluid) at the rear after the denser fluid had moved forward, and this mixed fluid increases in length with time [13]. However, it is generally known that gravity currents usually undergo either two or three distinct phases of flow: a slumping phase, self-similar phase and viscous phase. As also recorded by [12], that the instantaneous release of the two fluids after gate was removed led to an initial adjustment phase where the advancing head varies with constant velocity. Followed immediately by the second phase after the ambient fluid had reflected at the rear wall. This in turn overtakes the penetrating head of the current; only if the lock-exchange experiment was carried out in a finite confined channel [14]. At this point in the flow, it was observed that the penetrating head advances as $t^{2/3}$, but decreases with front speed as $t^{-1/3}$, where t is the time after which the gate was removed. Lastly, is the phase where viscous effects overcome inertial effects and the current front velocity decreases more rapidly as $t^{-4/5}$, with front position advancing as $t^{1/5}$ [1].

However, buoyancy reversal due to the nonlinear relation between temperature and density in water has also been a subject of extensive research recently; where the temperature dependence of water density is non-monotonic. In the case where water masses are on either side of the T_m come in contact by the instantaneous removal of the gate (lock-exchange), cabbeling is likely to occur even as the various fluids advance in their opposite directions. Such a lighter fluid is usually unsteady therefore, as it penetrates the ambient fluid there will be some degree of Rayleigh-Taylor instabilities which will lead to the production of denser fluid. During this process, any mixture that have mixed up to the T_m or a temperature closed to it will descend from the free surface to the floor even as the most buoyant fluid continue to spread outwards as surface gravity current [15, 16]. At this point, the mixed water which is denser than the original water masses will in turn spread outwards with a leading tip or head in the same direction as that of the surface current. Such that the ambient fluid is gradually replaced by this new produced denser current on the floor. Meanwhile, the ambient fluid exist at some point between the surface and the density current. But then, as time progresses, it is expected that fluid that have mixed up to T_m will continue to descend from the surface. While the nose or tip of the initial surface current will be arrested by cabbeling at much later time. So that only the density current will continue to spread outwards on the floor displacing the ambient fluid.

Surface gravity current resulting from warm discharge above the temperature of maximum density into ambient water below T_m was first investigated in the laboratory by Marmoush et al. [17], where mixing was found to be sufficiently

vigorous to eventually arrest the gravity current, after which a plume was observed to descend from the head of the arrested current. They were also able to obtain an empirical scaling law for the distance travelled by the surface current before arrest, but did not really give detailed description after the descending plume. Surface gravity current resulting from warm discharge into ambient water below T_m have also been investigated experimentally by Bukreev [18], and other detailed studies can also be found in [19 & 20].

In most of the previous experimental studies, the initial density difference was produced by the addition of salt. Whereas just a few have considered gravity current flows for which density variation is as a result of the change in the temperature (i.e., where either of the water masses is above or below T_m). The present investigation is based on numerical simulations that uses the lock exchange method as illustrated in Fig. 1, but with the assumption that density is a quadratic function of temperature. As such, the surface gravity current is expected to halt after the head might have entrained ambient fluid. And before the halting process, any part of the fluid that have mixed up to the T_m or a temperature close to it is expected to sink from the surface to the floor. Meanwhile, denser fluid that have descended to the floor will continue to spread as density current mixing further. We will vary the barrier position horizontally between $L/14$ and $5L/14$ for $\phi_{in} = 2.5$ on the right hand side. Meanwhile, on the left hand side, at position $13L/14$ and $9L/14$, $\phi_{in} = 0$, where L is the total length of the computational domain and ϕ_{in} , the initial temperature on the various sides of the barrier.

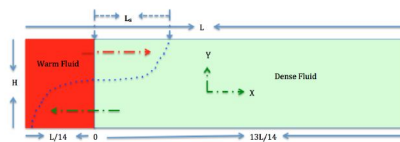


Fig. 1. Schematic presentation of Lock-exchange flow in a channel of length L and height H . The dotted line here gives the interface between the two fluids at some point in time after the release.

2 MODEL FORMULATION AND GOVERNING EQUATIONS

Behaviour of the surface gravity current as denser fluid undergo buoyancy reversal due to the nonlinear relation between density ρ and temperature T is key and as such, the following relation is appropriate for this investigation,

$$\rho = \rho_m - \beta(T - T_m)^2. \quad (2.1)$$

This, we believe gives a very good fit to the experimentally determined density of fresh water at temperatures below $10^\circ C$, if we consider $T_m = 3.98^\circ C$, $\rho_m = 1.000 \times 10^3 \text{ kg.m}^{-3}$ and $\beta = 8.0 \times 10^{-3} \text{ kg.m}^{-3}(\text{ }^\circ C)^{-2}$ [22, 23] and all other fluid properties (e.g. viscosity, thermal diffusivity) are assumed constant. We also assume that the flow is time dependent and two dimensional, and that the liquid property is constant except for the water density, which changes with temperature and in turn results to the buoyancy force. We can non-dimensionalise the coordinates x , y , velocity components u , v , time t , pressure p and temperature T by

$$U = \frac{u}{U_*} \quad V = \frac{v}{U_*} \quad X = \frac{x}{H} \quad Y = \frac{y}{H} \quad \tau = \frac{t}{\frac{H}{U_*}} \quad P = \frac{p}{\rho U_*^2} \quad \phi = \frac{T - T_\infty}{T_m - T_\infty}, \quad (2.2)$$

where x and u are horizontal, y and v are vertical; $U_* = \sqrt{\frac{\rho_\infty - \rho}{\rho} H}$ is the relative frontal velocity and domain height H . We also define dimensionless parameters, the Reynolds Re , Prandtl Pr and Froude Fr numbers, by

$$\nu = \frac{\mu}{\rho} \quad \alpha = \frac{k}{\rho c_p} \quad Re = \frac{U_* H}{\nu} \quad Pr = \frac{\nu}{\alpha} \quad Fr^2 = \frac{\rho_m U_*^2}{g\beta(T_m - T_\infty)^2 H}, \quad (2.3)$$

where ν and α are the respective diffusivities of momentum and heat, and μ is viscosity, k is thermal conductivity and c_p is specific heat capacity. In terms of these dimensionless variables and parameters, the continuity equation, the horizontal and vertical momentum equations and the thermal energy equation are given as

$$\frac{\partial U}{\partial X} + \frac{\partial V}{\partial Y} = 0 \quad (2.4)$$

$$\frac{\partial U}{\partial \tau} + U \frac{\partial U}{\partial X} + V \frac{\partial U}{\partial Y} = -\frac{\partial P}{\partial X} + \frac{1}{Re} \left(\frac{\partial^2 U}{\partial X^2} + \frac{\partial^2 U}{\partial Y^2} \right) \quad (2.5)$$

$$\frac{\partial V}{\partial \tau} + U \frac{\partial V}{\partial X} + V \frac{\partial V}{\partial Y} = -\frac{\partial P}{\partial Y} + \frac{1}{Re} \left(\frac{\partial^2 V}{\partial X^2} + \frac{\partial^2 V}{\partial Y^2} \right) + \frac{1}{Fr^2} [\phi^2 - 2\phi] \quad (2.6)$$

$$\frac{\partial \phi}{\partial \tau} + U \frac{\partial \phi}{\partial X} + V \frac{\partial \phi}{\partial Y} = \frac{1}{Re Pr} \left(\frac{\partial^2 \phi}{\partial X^2} + \frac{\partial^2 \phi}{\partial Y^2} \right) \quad (2.7)$$

Domain of the study is consists of a domain length L of total $L = 7000$, i.e., $0 \leq X \leq 7000$, and a domain height $H = 1000$ i.e., $0 \leq Y \leq 1000$. It is also important to mention here that the term L_s is use to describe the spread length of the surface gravity current.

Our initial conditions are an undisturbed, homogeneous medium,

$$U = 0, \quad V = 0, \quad \phi = 0, \quad \text{for } \tau < 0 \quad (2.8)$$

For $\tau \geq 0$ we have boundary conditions as follows. On the side walls:

$$U = 0, \quad V = 0, \quad \frac{\partial \phi}{\partial X} = 0 \quad (2.9)$$

At the plume source:

$$U = U_*, \quad V = 0, \quad \phi_{in} = 2.5 \text{ for } L/14 \text{ and } \phi_{in} = 0 \text{ for } 13L/14, \quad \text{for } X = 0, \text{ at } Y = H \quad (2.10)$$

On the floor of the domain:

$$U = 0, \quad V = 0, \quad \frac{\partial \phi}{\partial Y} = 0 \quad (2.11)$$

At the top of the domain:

$$\frac{\partial U}{\partial Y} = 0, \quad V = 0, \quad \frac{\partial \phi}{\partial Y} = 0 \quad (2.12)$$

The Reynolds number $Re = 500$, Froude number $Fr = 1$ and Prandtl number $Pr = 7$ will be fixed throughout this study. The dimensionless temperature $\phi_{in} = 2.5$ on $L/14$ is equivalent to a discharge at $10^\circ C$ into an ambient at $0^\circ C$. Numerical solution of the above equations is by means of COMSOL Multiphysics software. This commercial package uses a finite element solver with discretization by the Galerkin method and stabilisation to prevent spurious oscillations. We have used the "Extremely fine" setting for the mesh. Time stepping is by COMSOL's Backward Differentiation Formulas. Further information about the numerical methods is available from the COMSOL Multiphysics website [21]. Results will be illustrated mainly by surface temperature plots of dimensionless temperature on a colour scale from dark red for the ambient temperature $\phi = 0.0$, through yellow to white for the source temperature $\phi = 2.5$. Except at some point in the density current where we may have repeated temperature colour scale for a different temperature. Note that $\phi = 1.0$ corresponds to the temperature of maximum density while $\phi = 2.0$ is the temperature at which warm water has the same density as the ambient cold water.

3 RESULTS

The behaviour of warm discharge through lock-exchange in cold fresh water had just been investigated over the range of discharge temperature $2.5 \leq \phi_{in} \leq 6$, and for a fixed Reynolds number $Re = 500$, Froude number $Fr = 1$ and Prandtl number $Pr = 7$, and varied barrier position between $L/14$ and $5L/14$. However, the evolution of temperature field for $\phi_{in} = 2.5$ is shown in Figure 2, 3, 4 and 5, within the time range $0.1 \leq \tau \leq 300$

and $40 \leq \tau \leq 320$ respectively for effective analysis. Barrier position in the case as shown in Figure 2 and 3 is at $5L/14$, with $\phi_{in} = 2.5$ on the right hand side, and $\phi_{in} = 0$ on the left hand side. Meanwhile, the case as shown in Figure 4 and 5 is at $L/14$, with $\phi_{in} = 2.5$ on the right hand side, and $\phi_{in} = 0$ on the left hand side.

Within the first few time interval of the simulation, we observe the commencement of a cabbeling process at the point where the two water masses meet. This in turn had led to the production of insignificant amount of dense water (see Fig.2(b)), even as the lighter fluid on the right hand side began to override the ambient fluid forming surface current. But as time progresses, significant amount of denser fluid had descended to the floor. But then, the interaction between the ambient and the warm fluid had created an unstable interface (Rayleigh-Taylor instabilities), which ranges from the nose or head of the surface current to the rear (see Fig. 2(d)) even as the most buoyant fluid still penetrate further with a sharp head. However, the motion of this surface current decreases with time, while the mode of the unstable layer or the Rayleigh-Taylor instabilities increases with time (see Fig. 2(d) - (e), Fig. 3(f) - (g) and Fig. 4(b)). Within the process, we could also observe that the penetrating frontal head is always found to be replenished by a surface flow of warm unadulterated water from the rear, and this enables the current to penetrate further and also appeared to have maintained this sharp head as it advances (see Fig.4(b) - (e) and Fig. 5(f)).

During the flow, we could also observe that any vacuum created by the warmer fluid as it forms the surface current is always replaced by the

ambient fluid until the ambient fluid reflected at the left hand side wall and causes disruption at the rear of the frontal head (see Fig.3(h) & (i) and Fig.4(c)). It is clear that this single disruption has in turn intensifies the mixing rate at the rear, and this may also have caused a reduction in the motion of the current as the reverse reflected wave travel past the frontal head. This process also enabled a supply of warm water to the sinking zone (see Fig.3(h) & (i) and Fig.4(c)) as also recorded by Marmoush et al. [17]. However, mixing between the warm and the ambient fluid mostly occur at the interaction layer and any part that have mixed up to the T_m descending from the surface current (see Fig. 4(f) - (i)).

Meanwhile, as denser fluid became significant on the floor, it has also formed a density current with a sharp frontal head advancing in the same direction as that of the surface current (see Fig. 4(c) - (e) and Fig. 5(f) - (i)). To a certain length, we could also observe that the surface current had moved a much significant distance L_s (measured from the barrier position). The volume of this lighter water had reduced gradually and the velocity with which it travels with had also decreased almost to a halting state. This behaviour continued until the surface gravity current eventually halted, while the denser fluid continue to descend from different positions at the surface (see Fig.5(g) & (h)).

It is also becoming clear that denser fluid on the floor continue to spread outwards on the floor with a leading sharp head displacing the ambient fluid upwards (see Fig. 4(e) and Fig. 5(f) - (i)). It is also obvious that fluid in the density current is a mixture of different temperatures though, it is denser than both the ambient and the warm discharge. At much later time, development of Kelvin-Helmholtz instabilities was observed as density current advance towards the right hand side wall (see Fig. 6). However, this fluid will continue to flow as a density current as it mixes downstream until fluid density in the density current become the same as that of the ambient. In reality it is expected that all

the descending fluid will spread outwards on the floor mixing further to become the same density as the ambient fluid assuming the domain length is of countably infinite size or large enough to observe that. Thus, this is a limitation here as our domain of computation did not allow us to examine this scenario as density current mixes with ambient fluid downstream. But then, the development of Kelvin-Helmholtz instability as it penetrates further enables the denser water to blind very fast with the ambient.

Behaviour of the surface current is also shown for $\phi_{in} = 3, 4,$ and 6 in Figure 7, 8 and 9, where the first figure in each of the cases as shown in (Figure 7(a), 8(a) and 9(a)) shows the maximum penetration length L_s where the plume eventually halted. While, the (b) part show the advancement of the density current. However, the general behaviour in the results here is the same as described previously except for the quick advancement of the surface current to attain a greater penetration length within a short period before it eventually halted. Thus, the penetration length of the surface current increases with temperature, and decreases with time when compared with those in Fig. 2, 3, 4 & 5. The possible explanation to this might be that, plumes with the high temperature input possesses greater energy. Hence, such plumes could penetrate the ambient fluid faster to attain greater length within a short period, and this in turn enhances fast mixing rate that have led to entrainment of ambient fluid. This process also enhance quick production of denser fluid before the nose was finally arrested by cabbelling.

Whereas, those with the lower temperature input penetrate the ambient slowly, so they took longer time to mix. However, on the floor the denser fluid spread further outwards as a density current with a leading head with some degree of Kelvin-Helmholtz instabilities (see Fig.7(b)). Whereas, the current in Fig.8(b) and Fig.9(b) have not developed up to the stage as that in Fig.7(b)) within the simulation time.

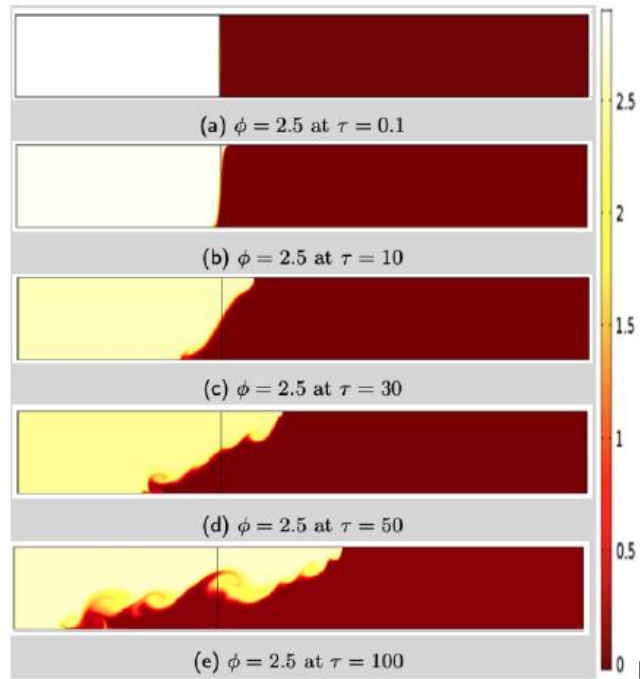


Fig. 2. Evolution of temperature field in the surface gravity current for $Fr = 1$ and Reynolds number $Re = 500$ with $\phi = 2.5$ at time $0.1 \leq \tau \leq 100$

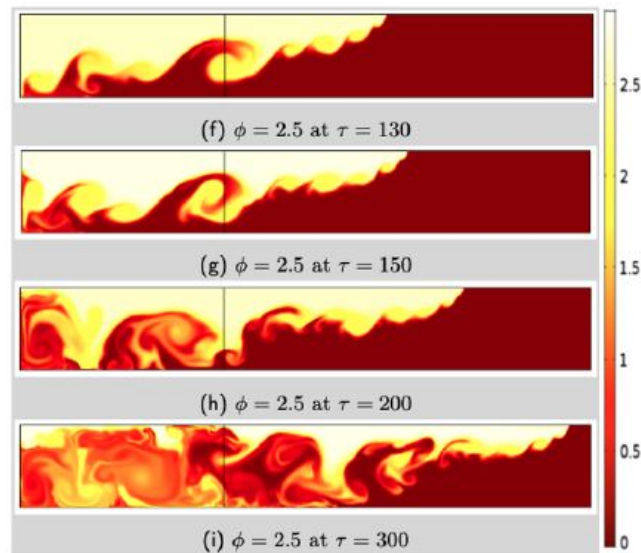


Fig. 3. Evolution of temperature field in the surface gravity current for $Fr = 1$ and Reynolds number $Re = 500$ with $\phi = 2.5$ at time $130 \leq \tau \leq 300$

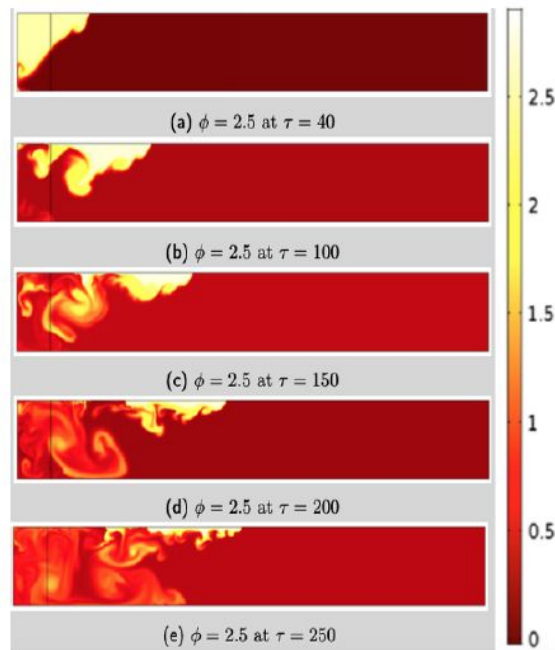


Fig. 4. Evolution of temperature field in the surface gravity current for $Fr = 1$ and Reynolds number $Re = 500$ with $\phi = 2.5$ at time $40 \leq \tau \leq 250$

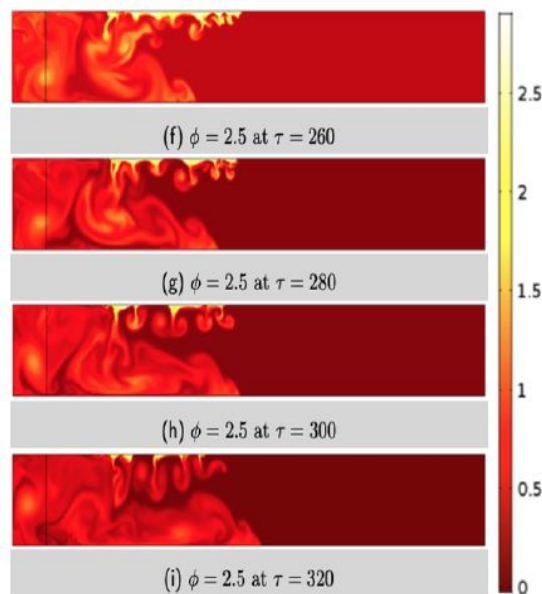


Fig. 5. Evolution of temperature field in the surface gravity current for $Fr = 1$ and Reynolds number $Re = 500$ with $\phi = 2.5$ at time $260 \leq \tau \leq 320$

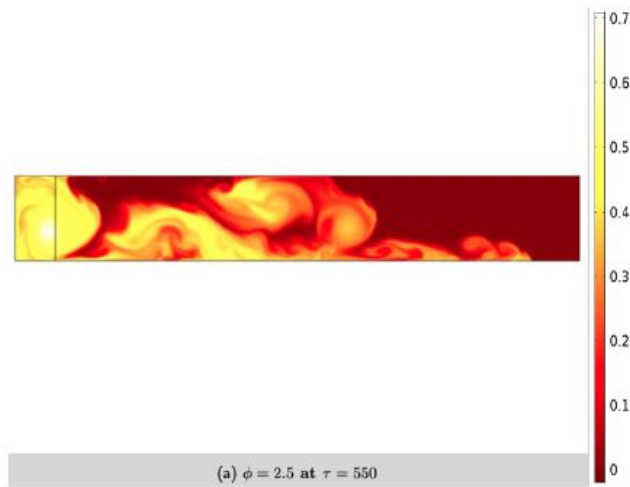


Fig. 6. Temperature field in the surface gravity current for $Fr = 1$ and Reynolds number $Re = 500$ with $\phi = 2.5$ at $\tau = 550$.

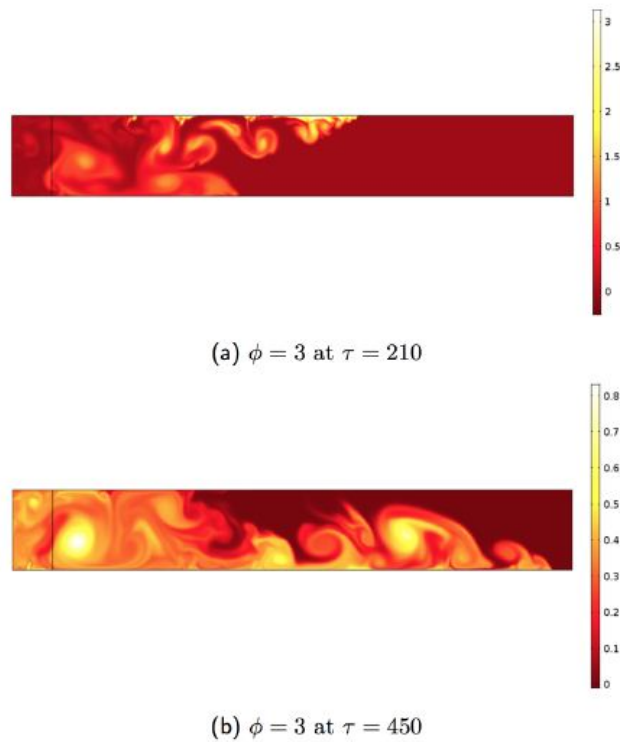


Fig. 7. Temperature field in the surface gravity current for $Fr = 1$ and Reynolds number $Re = 500$ with $\phi = 3$ at time 210 & 450

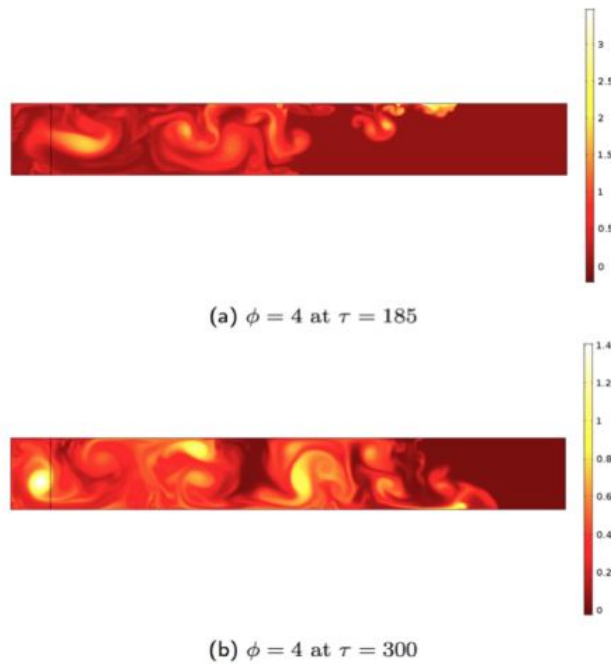


Fig. 8. Temperature field in the surface gravity current for $Fr = 1$ and Reynolds number $Re = 500$ with $\phi = 4$ at time 185 & 300

The behaviours as observed here in this paper also corresponds to some of the earlier experimental investigations by Marmoush et al. [17] and Bukreev [18]. For those by Bukreev [18], the author considered a discharge of temperature $\phi_{in} = 19.7^\circ C$, and the ambient temperature to be $\phi_{in} = 0.2^\circ C$. The author observed a vertical front immediately after the removal of the barrier in the form of thermal bar within the first 10 -12 seconds, and observe denser fluid sinking to the bottom. The quick production of denser fluid that sinks might be as a result of the little disturbance of the fluid during the gate removal. Whereas, we were also able to observe a cabbeling process at the start of the simulation but could not record denser fluid within this time. Apart from this difference, every other behaviour were also recorded by both Marmoush et al. [17] and Bukreev [18], only that Marmoush et al. [14] did not give detailed explanation on the density current as denser fluid get to the floor, neither did the authors record any cabbeling process which seemed to be a necessary event immediately after the gate removal.

Speed with which the frontal head of the surface current U_{ds} travels with time τ_n for plumes with $\phi_{in} = 2.5$ and 3 as represented by the blue and the red dots as shown in Figure 10. The advancement in the frontal head of the surface current is very different from the earlier description as given in the introduction that currents usually undergo either two or three distinct phases of flow: a slumping phase, self-similar phase and viscous phase [12, 14]. In such a scenario, it is expected that rate of decrease in velocity of the surface current occurs gradually, whereas in our investigation here, cabbeling process begins immediately the gate was removed. And as denser fluid at T_m is produced at every point in the surface current that sink to the floor due to cabbeling, this process caused a sudden decrease in velocity of the frontal head resulting to a quick halt. A similar behaviour were also recorded by Marmoush et al. [17]. However, Figure 10 show the case with a linear and logarithmic scale, where the relations that were drawn fit the case for a self-similar phase for the various ϕ_{in} values.

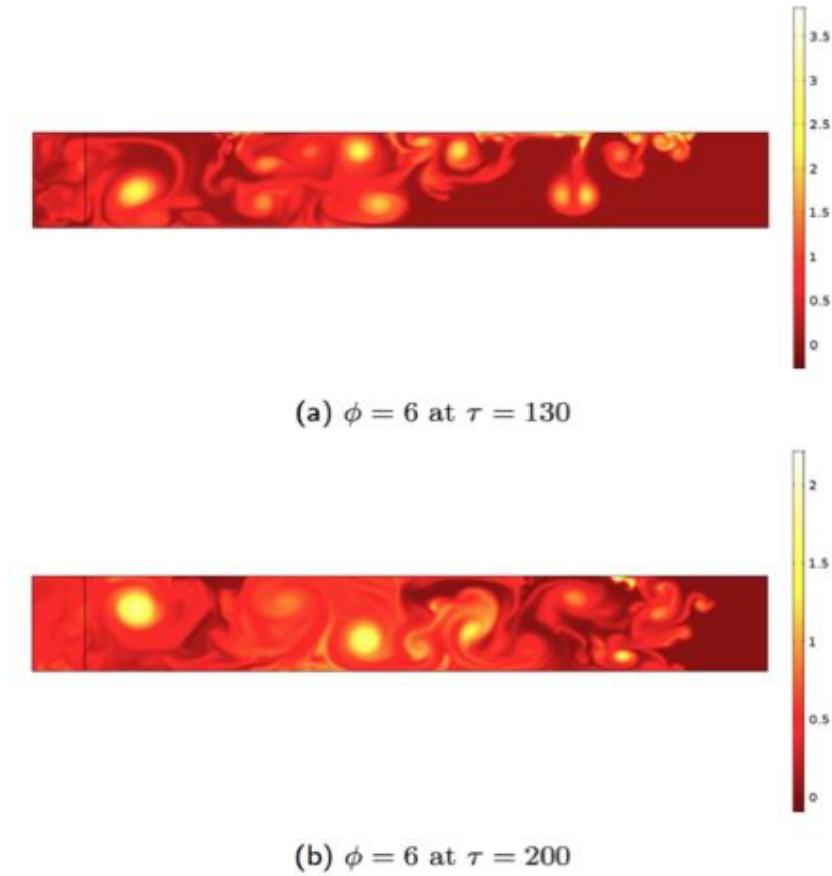


Fig. 9. Temperature field in the surface gravity current for $Fr = 1$ and Reynolds number $Re = 500$ with $\phi = 6$ at time 130 & 200

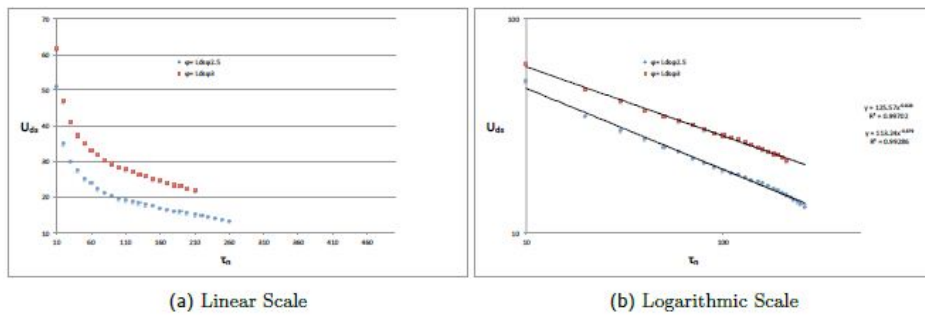


Fig. 10. Propagation speeds of the surface current U_{ds} for plumes with discharge temperature $\phi_{in} = 2.5$ & 3 with respect to time τ_n .

Therefore, a single regime could be identified from the various plots, and shown as a fairly straight line that represents the best fit power laws obtained by linear regression of $\log U_{ds}$ vs $\log \tau_n$ for $\phi_{in} = 2.5$ and 3:

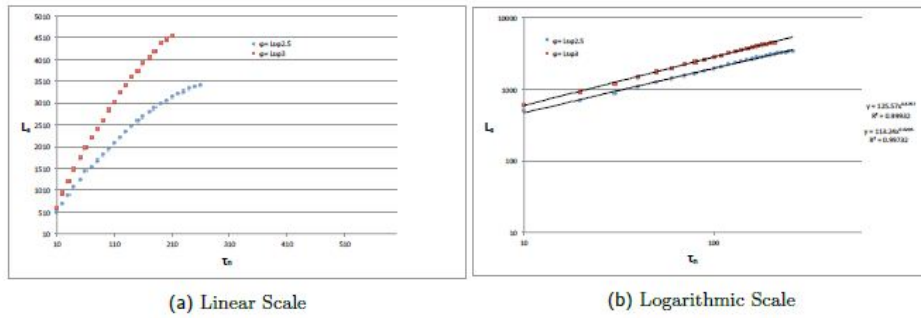


Fig. 11. Variation of spreading distance of the surface current L_s for plumes with discharge temperature $\phi_{in} = 2.5$ & 3 with respect to time τ_n .

$$U_{ds} = 113.24\tau_n^{-0.379} \quad [R^2 = 0.993] \quad (3.1)$$

for $\phi_{in} = 2.5$, and

$$U_{ds} = 125.57\tau_n^{-0.323} \quad [R^2 = 0.997] \quad (3.2)$$

for $\phi_{in} = 3$, where R^2 is the regression coefficient in each case.

Result with the linear scale as shown in Fig.10(a) also looks similar to those by Bukreev [18], where the author have considered the speed of the surface current at different barrier position. Furthermore, Fig.11 also show empirically determined spread length L_s of the surface current measured from the barrier position to the point where the surface current eventually halted and plotted against time τ_n for the various $\phi_{in} = 2.5$ and 3.

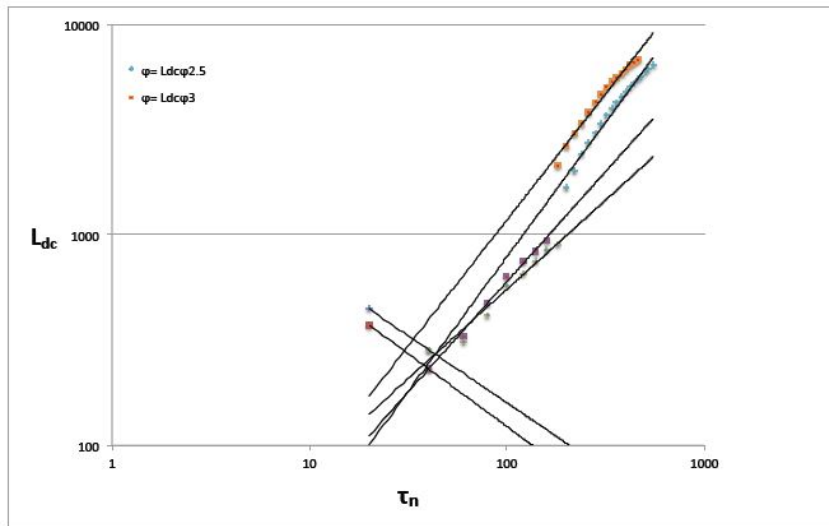


Fig. 12. Variation of spreading distance of the density current L_{dc} for plumes with discharge temperature $\phi_{in} = 2.5$ & 3 with respect to time τ_n .

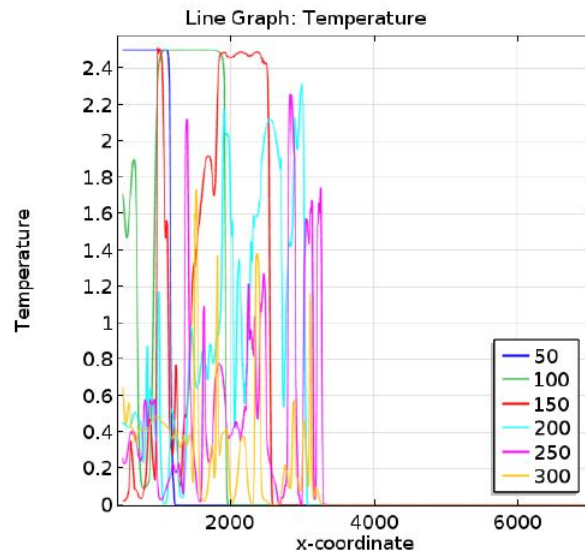


Fig. 13. Dimensionless temperature profiles at some point close to the surface $\phi(X, 900)$ at time $\tau = 50, 100, 150, 200, 250, 300$ for plumes with $Re = 500, Pr = 7, \phi_{in} = 2.5$ and for $Fr = 1$

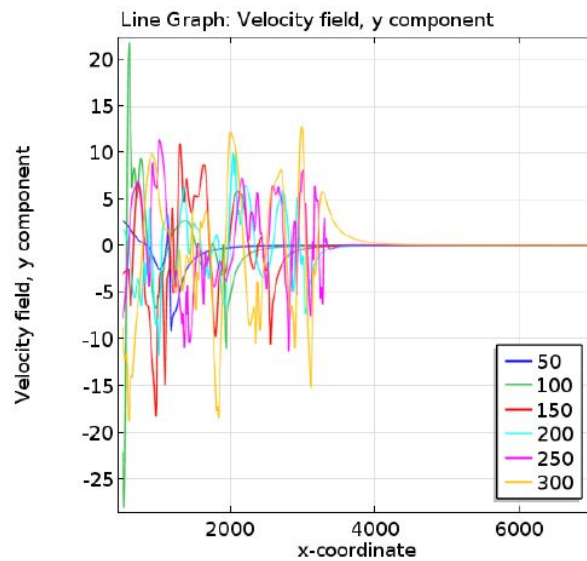


Fig. 14. Dimensionless vertical velocity profiles at some point close to the surface $V(X, 900)$ at time $\tau = 50, 100, 150, 200, 250, 300$ for plumes with $Re = 50, Pr = 7, \phi_{in} = 2.5$ and for $Fr = 1$

Result with the linear scale as shown in Fig.11(a) also looks similar to those by Bukreev [18], as the author considered the spread length of the surface current at different barrier position. However, in our result here, a single regime could be identified in this case from the various plots as shown in Fig.11(b). Where it is shown as a straight line that represents the best fit power laws obtained by linear regression of $\log L_s$ on $\log \tau_n$ for $\phi_{in} = 2.5$ and 3:

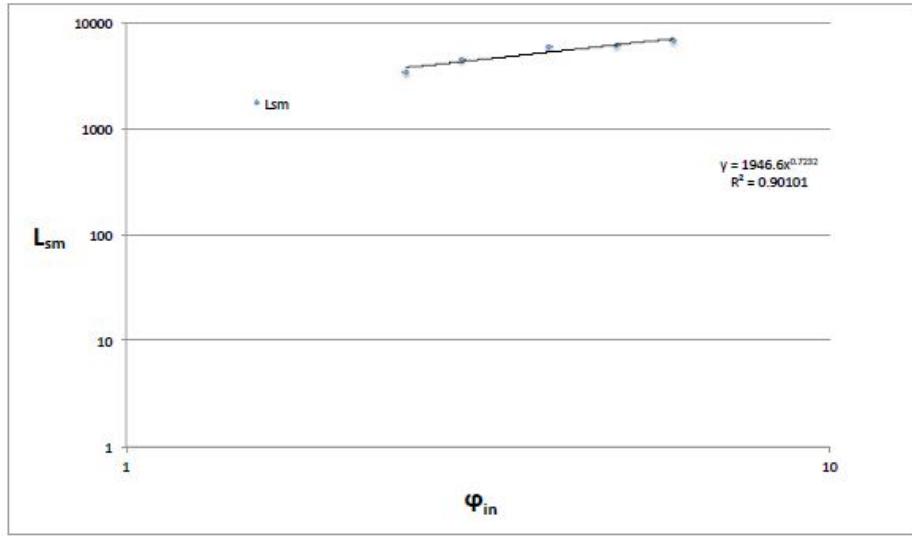


Fig. 15. Plot of the final spread length of the surface current L_{sm} as a function of ϕ_{in} .

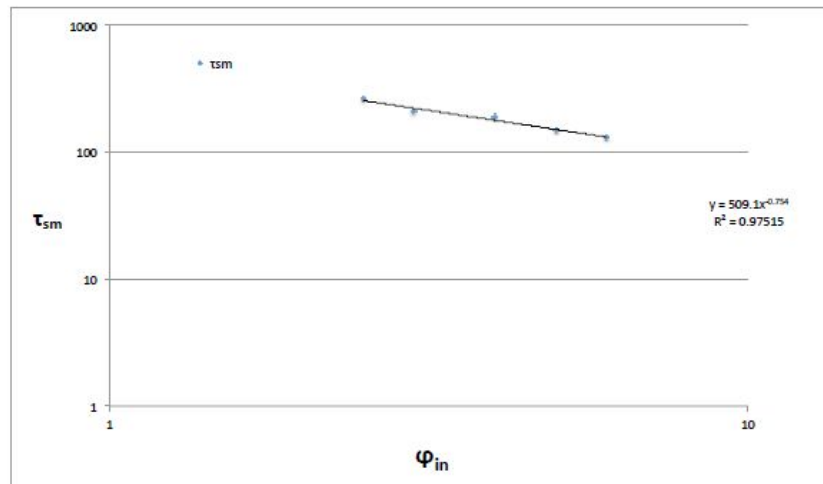


Fig. 16. Plot of the Time taken to reach the final spread length of the surface current τ_{sm} as a function of ϕ_{in} .

$$L_s = 113.24\tau_n^{0.621} \quad [R^2 = 0.997] \quad (3.3)$$

for $\phi_{in} = 2.5$, and

$$L_s = 125.57\tau_n^{0.677} \quad [R^2 = 0.999] \quad (3.4)$$

for $\phi_{in} = 3$.

We have also considered the spreading behaviour of the density current L_{dc} on the floor, and this is

shown in Figure 12. for $\phi_{in} = 2.5$ and 3 as represented by the blue and red dotted lines. The density current here is described in three distinct phases, where the first phase is between $\tau_n = 20$ and 40. At this point, we observe a cabbelling process at the initial time interval of the simulation together with a slumping phase that have led to the production of insignificant amount of denser fluid descending to the floor. This fluid began to flow in the same direction as that of the surface current, but then, the flow of this denser fluid on the floor was disrupted by the slumping phase being that its volume was small. Thus, this behaviour resulted to a decrease in its spread length as warmer fluid move upwards, trying to override the ambient fluid. After wards is the second phase which occurs within the time range $\tau_n = 40$ & 160 for $\phi_{in} = 3$, and $\tau_n = 40$ & 180 for $\phi_{in} = 2.5$. Within this phase, it was observed that the deflection of ambient fluid on the left hand side wall after the slumping phase enhances vigorous mixing, leading to quick production of denser fluid with a leading head as significant amount of denser fluid was produced. Whereas, the last phase occurs as denser fluid from different position at the surface descends to the floor, linking the initial leading head. This behaviour now led to a sudden increase in the density current. This observation was made within the time range $\tau_n = 180$ & 440 for $\phi_{in} = 3$, and $\tau_n = 200$ & 550 for $\phi_{in} = 2.5$. Therefore, we could identify three phases in the various ϕ_{in} cases as shown in Fig.12. Relations are also drawn that describe these different phases (spreading distance L_{dc}) as a function of time for both cases. Thus, this is shown by the lines in Fig.12, which represent best fit power laws obtained by linear regression of $\log L_{dc}$ on $\log \tau_n$ in table 1 and 2.

Table 1: Relations describing the spread length of the density current L_{dc} on the floor as a function of time τ_n for $\phi = 3$

| Phase | $L_n\phi 3$ formula | Error $L_n\phi 3$ |
|-------|-------------------------------|-------------------|
| 1st | $\approx 2982.2\tau^{-0.692}$ | $\approx \pm 0$ |
| 2nd | $\approx 4.817\tau^{1.048}$ | ≈ 0.175 |
| 3rd | $\approx 4.728\tau^{1.199}$ | ≈ 0.290 |

Table 2: Relations describing the spread length of the density current L_{dc} on the floor as a function of time τ_n for $\phi = 2.5$

| Phase | $L_n\phi 2.5$ formula | Error $L_n\phi 2.5$ |
|-------|-------------------------------|---------------------|
| 1st | $\approx 3005\tau^{-0.637}$ | $\approx \pm 0$ |
| 2nd | $\approx 11.094\tau^{0.8485}$ | ≈ 0.138 |
| 3rd | $\approx 2.1776\tau^{1.2792}$ | ≈ 0.286 |

Profiles of temperature and vertical velocity component on the surface gravity current at the height $Y = 900$ at some distance below the surface were examined, so as to get more information on the spreading behaviour of the current. This is shown in Figure13 and Figure.14, for $\phi = 2.5$. It is clear from the profile of temperature (Fig.13) that there was intense mixing at that level except at $\tau = 50$ where a very warm fluid was observed up to a significant distance. When examined properly, we can again notice that most of the fluid within the time range $200 \leq \tau \leq 300$ is already dense right at the barrier position. Thus, we can say in general that, temperature decreases rapidly with time at that level. With discharge temperature $\phi = 2.5$, the plume just required little mixing to attain the same density as that of the ambient. The fluctuations in the temperature profiles also confirm that decrease in temperature with horizontal length is not monotonic. In a similar manner, we can also confirm from the profiles of vertical velocity (Fig.14) that there is a lot of upwards and downwards movement of the fluid at that level. Where the downwards velocities as recorded indicates the process where fluid that have mixed up to a temperature $\phi < 2$ starts to sink at that level. Similar downwards velocities were also recorded by George & Kay [15] at some point close to the surface when the authors considered plumes that impinge on a ceiling through warm discharge.

Lastly, we have also considered plots of the final spread length of the surface current L_{sm} and the time taken to reach that final spread length τ_{sm} as a function of ϕ_{in} as shown in Figure 15 and 16. As we have explained previously that the advancement of the most buoyant fluid is always quicker and as such attain a greater penetration length within a short period before being arrested by cabbelling.

Thus, the penetration length of the surface current increases with temperature, and decreases with time and this is evident in Figure 15 and 16. Therefore, a single regime was identified from the various plots, and shown as a straight line that represents the best fit power laws obtained by linear regression of both $\log L_{sm}$ and $\log \tau_{sm}$ on $\log \phi_{in}$:

$$L_{sm} = 1946.6\phi_{in}^{0.723} \quad [R^2 = 0.901] \quad (3.5)$$

for $\phi_{in} = 2.5$, and

$$\tau_{sm} = 509.1\phi_{in}^{-0.754} \quad [R^2 = 0.975] \quad (3.6)$$

for $\phi_{in} = 3$, where R^2 is the regression coefficient in each case.

4 CONCLUSION

We have thoroughly investigated the behaviour of warm discharge through lock exchange, with the assumption that density was taken as a quadratic function of temperature. However, our results here are very similar to the experimentally studied cases by Marmoush et al. [17] and Bukreev [18], where we observe high level of Rayleigh-Taylor instabilities as warm water penetrate the ambient fluid as surface current. A process where fluid that have mixed up to T_m or a temperature close to it descending from the surface current due to cabbeling were also observe. In our investigation here, we were unable to observe the slumping phase and the viscous phase as described in most of the earlier investigations [12, 14], when considering speed with which the frontal head of the surface current U_{ds} travels with as a function of time. This is due to the fact that cabbeling process begins immediately we assume gate removal. And as denser fluid at T_m is produced at every point in the surface current that sink to the floor due to cabbeling, this process causes a sudden decrease in velocity of the frontal head right from the start of the simulation, and this in turn resulting to a quick halt of the surface current. Though, both Marmoush et al. [17] and Bukreev [18] did not obtain a relation that describe the rate of spread of the surface current. Whereas, we were able to provide relation that fit the case for a self-similar phase for the various ϕ_{in} values as given in equation (13) and (14). Relations were also drawn that describes spread length of both the surface and density current as a function of time, and this is given in equation (15) and (16) and in table 1 & 2. Relation that describe the final spread length of the surface current L_{sm} and the

time taken to reach that final spread length τ_{sm} as a function ϕ_{in} are also given in equation (17) and (18), where it shows that penetration length of the surface current increases with temperature, and decreases with time and this is evident in Figure 15 and 16.

Lastly, we also observed that denser fluid on the floor had filled some given section of the domain (see Figure 6) but with a leading front together with some degree of Kelvin-Helmholtz instabilities immediately after the penetrating tip. It is ideal to make clear here that the fluid which seemed to have filled section of the domain is still part of the descending denser fluid, and it is expected of such fluid to spread outwards as density current. As also stated earlier, all of this denser fluid in reality will continue to spread outwards on the floor as density current mixing further to become the same density as that in the ambient assuming that the domain of computation is of greater length. Thus, this is a limitation here and have also restricted us from observing the full possible behaviour of the development of Kelvin-Helmholtz instability as τ take greater values.

This work as presented here is practical and relevant to many fields of study and also enhances policy making towards the protection of the aquatic ecosystems. We know that this irregular behaviour in the property of water is the primary cause for a number of phenomena such as the formation of: thermal bar, fountains, gravity currents, etc. These behaviours are mostly found in lakes, especially in holomictic lakes, and in the area where the two water masses meet, the mixing line of the water at the contact zone forms a descending plume that draws in surrounding water, causing a sharp thermal front.

Another practical source for which such behaviour could be found is in the disposal of waste water from power generating plant. It is a known fact thermoelectric power generating plants are known to have been using a large amount of water which was estimated to be of about 201 billion gallons per day mostly used for cooling. There are three basic types of cooling systems namely; once-through, closed-cycle, and dry cooling. The once-through cooling pattern is known to be the most water-intensive and the cause of the most severe environmental impacts, such as the killing of billions of fish, degrading aquatic ecosystems, and increasing the temperature of our rivers, lakes, and ocean waters by about 8 to 12C once its warm discharge is released downstream.

Furthermore, if the ambient water is not deep enough, there is also the possibility that the plume could rise to the surface quickly and still be positively buoyant, where it spreads outwards as a surface gravity current, cooling further by entrainment and possibly by losing heat to the atmosphere: then cabbelling is bound to occur in the surface gravity current and any mixture that has either mixed to the temperature of maximum density or to a temperature close to it will sink forming a fountain. As a matter of fact, when any of these means of thermal pollution are situated close to natural water bodies, the discharge of such warm water may definitely give rise to environmental problems; where the sudden increase in the water temperature after discharge also leads to "thermal shock" killing aquatic life that has become acclimatised to living in a stable temperate environment. Thus, researchers can carryout more investigations on the biological aspect of it

COMPETING INTERESTS

Authors have declared that no competing interests exist.

REFERENCES

- [1] Nogueira ISH, Adduce C, Alves E, France JM. Analysis of Lock-exchange

- gravity currents over smooth and rough beds. *Journal of Hydraulic Research*. 2013;51(4):417-531.
- [2] Ozan YA, Constantinescu G, Hogg JA. Analysis of Lock-exchange gravity currents Propagating in a channel containing an array of obstacles. *Journal of Fluid Mechanics*. 2015;765:544-575.
- [3] Cenedese C, Nokes R, Hyatt J. Lock-exchange gravity currents over rough bottoms. *Journals of Environmental Fluid Mechanics*; 2016. DOI: 10.1007/s10652-016-9501-0
- [4] Belcher SE, Harman IN, Finnigan JJ. The wind in the willows: flows in forest canopies in complex terrain. *Annu. Rev. Fluid Mechanics*. 2012;44:479-504.
- [5] Finnigan J. Turbulence in plant canopies. *Annu. Rev. Fluid Mechanics*. 2000;32(1):519-571.
- [6] Britter R, Hanna S. Flow and dispersion in urban areas. *Annu. Rev. Fluid Mechanics*. 2003;35(1):469-496.
- [7] Huq P, White LA, Carrillo A, Redondo J, Dharmavaram S, Hanna SR. The shear layer above and in urban canopies. *Journal of Appl. Meteorol. Climatol*. 2007;46(3):368-376.
- [8] Nepf HM. Flow and transport in regions with aquatic vegetation. *Annu. Rev. Fluid Mechanics*. 2012;44(1):123-142.
- [9] Fay AJ. The Spread of Oil Slicks on a Calm Sea. In: Houtl D. P., ed. *Oil on the Sea*, Plenum Press, New York. 1969;53-63.
- [10] Fannelop TK, Waldman GD. Dynamics of oil slicks. *AIAA Journal*. 1972;10(4):506-510.
- [11] Houtl DP. Oil spreading on the sea. *Annu. Rev. Fluid Mechanics*. 1972;4:341-368.
- [12] Huppert HE, Simpson JE. The slumping of gravity currents. *Journal of Fluid Mechanics*. 1980;99:785-799.
- [13] Hacker J, Linden FP, Dalziel BS. Mixing in lock-release gravity currents. *Dynamics of Atmospheres and Oceans*. 1996;24:183 - 195.
- [14] Rottman JW, Simpson JE. Gravity currents produced by instantaneous releases of a heavy fluid in a rectangular channel. *Journal of Fluid Mechanics*. 1983;135:95-110.

- [15] George MA, Kay A. Numerical simulation of a line plume impinging on a ceiling in cold fresh water. *International Journal of Heat and Mass Transfer*. 2017;108:1364-1373.
- [16] Foster TD. An analysis of the Cabbeling instability in Sea water. *Journals of Physical Oceanography*. 1972;2(3):294-301.
- [17] Marmoush YR, Smith AA, Hamblin PF. Pilot experiments on thermal bar in lock exchange flow. *Journal of Energy Engineering*. 1984;110(3):215-227.
- [18] Bukreev IV. Effect of the nonmonotonic temperature dependence of water density on the propagation of a vertical plante jet. *Journal of Applied Mechanics and Technical Physics*. 2006;47(2):169-174.
- [19] Bukreev IV. Effect of the anomalous temperature dependence of water density on surface gravity current. *Journal of Applied Mechanics and Technical Physics*. 2005;46(1):49-54.
- [20] Bukreev IV. Effect of the nonmonotonic temperature dependence of water density on the decay of an initial discontinuity. *Journal of Applied Mechanics and Technical Physics*. 2006;47(1):54-60.
- [21] COMSOL Multiphysics Cyclopedia. The Finite Element Method (FEM). [ONLINE]. Available:<https://www.comsol.com/multiphysics/finite-element-method> Accessed 28 April 2016
- [22] Moore DR, Weiss NO. Nonlinear penetrative convection. *Journal of Fluid Mechanics*. 1973;61:553-581.
- [23] Oosthuizen PH, Paul JT. A Numerical study of the Steady State Freezing of Water in an open Rectangular Cavity. *International Journal of Numerical Methods for Heat and Fluid Flow*. 1996;6(5):3-16.

© 2022 George and Kay; This is an Open Access article distributed under the terms of the Creative Commons Attribution License (<http://creativecommons.org/licenses/by/4.0>), which permits unrestricted use, distribution and reproduction in any medium, provided the original work is properly cited.

Peer-review history:
The peer review history for this paper can be accessed here:
<https://www.sdiarticle5.com/review-history/83005>